Combining ptychographical algorithms with the Hybrid Input-Output (HIO) algorithm

Konijnenberg, A. P.; Coene, W. M J; Pereira, S. F.; Urbach, H. P.

DOI
10.1016/j.ultramic.2016.08.020

Publication date
2016

Document Version
Final published version

Published in
Ultramicroscopy

Ultramicroscopy 171 (2016) 43–54

Contents lists available at ScienceDirect

Ultramicroscopy

journal homepage: www.elsevier.com/locate/ultramic

Combining ptychographical algorithms with the Hybrid Input-Output (HIO) algorithm

A.P. Konijnenberg [a,*], W.M.J. Coene [a,b], S.F. Pereira [a], H.P. Urbach [a]

[a] Optics Research Group, Delft University of Technology, Delft 2628 CH, Netherlands
[b] ASML Netherlands B.V., De Run 6501, 5504 DR Veldhoven, The Netherlands

ARTICLE INFO

Article history:
Received 7 April 2016
Received in revised form
22 July 2016
Accepted 29 August 2016
Available online 31 August 2016

Keywords:
Ptychography
Phase retrieval

ABSTRACT

In this article we combine the well-known Ptychographical Iterative Engine (PIE) with the Hybrid Input-Output (HIO) algorithm. The important insight is that the HIO feedback function should be kept strictly separate from the reconstructed object, which is done by introducing a separate feedback function per probe position. We have also combined HIO with floating PIE (fPIE) and extended PIE (ePIE). Simulations indicate that the combined algorithm performs significantly better in many situations. Although we have limited our research to a combination with HIO, the same insight can be used to combine ptychographical algorithms with any phase retrieval algorithm that uses a feedback function.

1. Introduction

In coherent diffractive imaging (CDI) the goal is to reconstruct an object from intensity measurements that are obtained in the far field. Mathematically, we want to reconstruct a complex-valued object transmission function $O(\mathbf{r})$ by illuminating it with a probe $P(\mathbf{r})$ and measuring in the far field the intensity $|\Psi(\mathbf{k})|^2 = |\mathcal{F}\{P(\mathbf{r})O(\mathbf{r})\}|^2$. Here, $\mathbf{r}$ and $\mathbf{k}$ are 2D position vectors in real space and reciprocal (Fourier) space respectively. To achieve this, many iterative phase retrieval methods have been developed such as the Error Reduction (ER) algorithm [1], the Hybrid Input-Output (HIO) algorithm [2], the Solvent Flipping (SF) algorithm [3], the Averaged Successive Reflections (ASR) algorithm [4], the Hybrid Projection Reflection (HPR) algorithm [5], or the Relaxed Averaged Alternating Reflectors (RAAR) algorithm [6]. These algorithms aim to reconstruct with a single intensity measurement.

A somewhat different type of algorithm is used for ptychography. In this case we do not take just one intensity measurement, but we displace the probe by some vector $\mathbf{R}$, and for multiple different $\mathbf{R}$'s we obtain the intensity patterns $|\Psi(\mathbf{k}, \mathbf{R})|^2 = |\mathcal{F}\{P(\mathbf{r}-\mathbf{R})O(\mathbf{r})\}|^2$. The probe $P(\mathbf{r})$ and the probe positions $\mathbf{R}$ are chosen such that there is sufficient overlap between the probes at different positions. This is illustrated in Fig. 1(a). The redundant measured information due to the overlap allows for a successful reconstruction. Non-iterative ptychographical methods have been developed [7–9], though here we will focus on the iterative ptychographical reconstruction methods. The algorithm used to reconstruct $O(\mathbf{r})$ in ptychography is usually the Ptychographical Iterative Engine (PIE) [10], although it has been expanded in various ways. For example, to reconstruct simultaneously an unknown object $O(\mathbf{r})$ and an unknown probe $P(\mathbf{r})$, the Extended Ptychographical Iterative Engine (ePIE) has been developed [11], as well as a nonlinear optimization approach [12]. In case we want to reconstruct $O(\mathbf{r})$, but the intensity measurements are undersampled, the Floating Ptychographical Iterative Engine (fPIE) can be used [13].

Upon examining PIE, one could conclude that it is in a sense an extension of the ER algorithm, because in an iteration of PIE, for each probe position $\mathbf{R}$ the guessed object $O_g(\mathbf{r})$ is updated only in the region where $P(\mathbf{r})$ is non-zero, while the rest of the guessed object remains unchanged. It has been known however that HIO outperforms ER [14,15], so it makes sense to redesign PIE as an extension of HIO instead of as an extension of ER. It is shown in [14] that ER is a steepest-descent gradient search algorithm, which is known to be the weakest gradient-based nonlinear optimization algorithm. Indeed, phase retrieval methods other than ER have been adapted to ptychography [16,17]. However, the precise way in which we adapt these methods to ptychography matters significantly, as we show in this article.

The difference between ER and HIO is the following: suppose our object $O(\mathbf{r})$ has a known finite support S. In its complement S^c, we know that $O(\mathbf{r}) = 0$. In the ER scheme, the guessed object $O_g(\mathbf{r})$ is set to 0 for all $r \notin S$ at each iteration. In the HIO scheme, the guessed object $O_g(\mathbf{r})$ is not set to 0 for all $r \notin S$, but rather it is set to some feedback function. If one happens to have a non-negativity

* Corresponding author.
E-mail address: a.p.konijnenberg@tudelft.nl (A.P. Konijnenberg).

http://dx.doi.org/10.1016/j.ultramic.2016.08.020

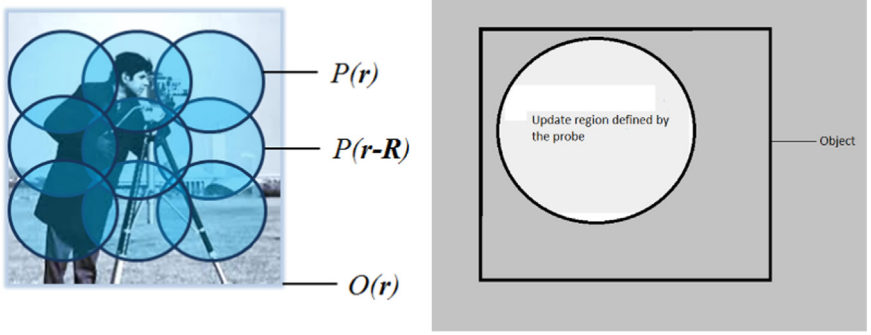

Fig. 1. Left: an illustration of ptychography. An object $O(\mathbf{r})$ is illuminated by a probe $P(\mathbf{r})$ that is shifted over different vectors $\mathbf{R}$. For each probe position, the intensity of the diffraction pattern $|\Psi(\mathbf{k})|^2 = |\mathcal{F}\{P(\mathbf{r}-\mathbf{R})O(\mathbf{r})\}|^2$ is measured. These measurements are then used to reconstruct the object $O(\mathbf{r})$. Right: an illustration of the HIO feedback function. For ptychography, the feedback function lies outside the support of the probe.

constraint (which is problem dependent), then this feedback function can also be applied in the points in S where the updated guessed exit wave violates this constraint.

In the case of ptychography, if we assume the probe $P(\mathbf{r})$ to be a step function for simplicity, the support S for each measurement is defined by $P(\mathbf{r})$. Thus, the support of the feedback is complementary to the probe, and not complementary to the object as in regular HIO (see Fig. 1(b)). One should therefore take caution when introducing the feedback function as described in HIO: while in normal HIO we can store a feedback function in the complement of S, in ptychography we cannot do this since $O_g(\mathbf{r})$ already is defined there. In case the object itself has a finite support S_O and some probes scan outside this support, then it may be possible to apply a feedback function in the complement of S_O. However, in our simulation we will not consider this scenario.

While it has already been suggested to combine PIE with other phase retrieval algorithms such as HIO and RAAR [16], they allow the feedback function to overlap with the object estimate $O_g(\mathbf{r})$. We propose here an alternative version of HIO combined with PIE where the feedback function is kept strictly separated from the object. We study how this method can be extended to HIO-fPIE and HIO-ePIE, and compare our method to the other reconstruction algorithms.

2. Theory

In this section we describe the four different algorithms that we will compare. Sequential PIE describes the regular PIE algorithms where the guessed object is updated one probe position at a time [10]. In *sequential* HIO-PIE, our newly proposed algorithm, we also update the guessed object one probe position at a time, but at the same time we have a feedback function (as in HIO) per probe position to improve the convergence. We also describe *simultaneous* (HIO-)PIE as suggested by [16], where the guessed object is updated for all probe positions at once.

Sequential PIE:

1. We start with the n^{th} guessed object $O_{g,n}(\mathbf{r})$.
2. For a certain probe position $\mathbf{R}$ we calculate the guessed exit wave $\psi_{g,n}(\mathbf{r},\mathbf{R}) = O_{g,n}(\mathbf{r})P(\mathbf{r}-\mathbf{R})$.
3. We calculate the guessed diffracted field $\Psi_{g,n}(\mathbf{k},\mathbf{R}) = \mathcal{F}\{\psi_{g,n}(\mathbf{r},\mathbf{R})\}$.
4. We replace the amplitude of the guessed diffracted field $\Psi_{g,n}(\mathbf{k},\mathbf{R})$ with the measured amplitude of the diffracted field $\Psi(\mathbf{k},\mathbf{R})$, while keeping the phase of $\Psi_{g,n}(\mathbf{k},\mathbf{R})$. This gives the corrected guessed diffracted field $\Psi_{c,n}(\mathbf{k},\mathbf{R}) = \frac{\Psi_{g,n}(\mathbf{k},\mathbf{R})}{|\Psi_{g,n}(\mathbf{k},\mathbf{R})|}|\Psi(\mathbf{k},\mathbf{R})|$.
5. We obtain a corrected guess for the exit wave function by inverse Fourier transforming the corrected guess of the diffracted field $\psi_{c,n}(\mathbf{r},\mathbf{R}) = \mathcal{F}^{-1}\{\Psi_{c,n}(\mathbf{k},\mathbf{R})\}$.
6. We update the guess of the object in the region where the probe $P(\mathbf{r}-\mathbf{R})$ is sufficiently strong:

$$O_{g,n}(\mathbf{r}) := \begin{cases} \psi_{c,n}(\mathbf{r},\mathbf{R})\dfrac{P^*(\mathbf{r}-\mathbf{R})}{|P(\mathbf{r}-\mathbf{R})|^2} & \text{if } |P(\mathbf{r}-\mathbf{R})| \geq \alpha, \\ O_{g,n}(\mathbf{r}) & \text{if } |P(\mathbf{r}-\mathbf{R})| < \alpha. \end{cases} \tag{1}$$

Here, α is a small parameter to prevent errors from blowing up such where $|P(\mathbf{r}-\mathbf{R})|$ is small. α should be chosen sufficiently small so the entire object is covered by the update regions. Once we have done this for all probe positions $\mathbf{R}$, one iteration is completed and we can set $O_{g,n+1}(\mathbf{r}) = O_{g,n}(\mathbf{r})$.

Sequential HIO-PIE:

1. We start with the n^{th} guessed object $O_{g,n}(\mathbf{r})$, and the n^{th} feedback function $B_n(\mathbf{r},\mathbf{R})$ for probe position $\mathbf{R}$. The initial value of the feedback function is $B_0(\mathbf{r},\mathbf{R}) = 0$.
2. For a certain probe position $\mathbf{R}$ we calculate the guessed exit wave $\psi_{g,n}(\mathbf{r},\mathbf{R}) = O_{g,n}(\mathbf{r})P(\mathbf{r}-\mathbf{R})$.
3. We calculate the guessed diffracted field $\Psi_{g,n}(\mathbf{k},\mathbf{R}) = \mathcal{F}\{\psi_{g,n}(\mathbf{r},\mathbf{R}) + B_n(\mathbf{r},\mathbf{R})\}$.
4. We obtain a corrected guess for the exit wave function $\psi_{c,n}(\mathbf{r},\mathbf{R})$ as in steps 4–5 of Sequential PIE.
5. We update the feedback function in the region where the probe is sufficiently weak:

$$B_{n+1}(\mathbf{r},\mathbf{R}) = \begin{cases} 0 & \text{if } |P(\mathbf{r}-\mathbf{R})| \geq \alpha, \\ B_n(\mathbf{r},\mathbf{R}) - \beta\psi_{c,n}(\mathbf{r},\mathbf{R}) & \text{if } |P(\mathbf{r}-\mathbf{R})| < \alpha. \end{cases} \tag{2}$$

β is the HIO feedback parameter which we choose to be 0.9.
6. We update the guess of the object as in Sequential PIE according to Eq. (1).

Simultaneous PIE:

1. We have a guess for the exit wave functions $\psi_{g,n}(\mathbf{r},\mathbf{R}_j)$ for all probe positions $\mathbf{R}_j$.
2. We calculate the corrected guess for the exit wave functions $\psi_{c,n}(\mathbf{r},\mathbf{R}_j)$ for all probe positions $\mathbf{R}_j$ using steps 3–5 of Sequential PIE.
3. We obtain new estimates for the exit wave functions using

$$\psi_{g,n+1}(\mathbf{r},\mathbf{R}_j) = P(\mathbf{r}-\mathbf{R}_j)\frac{\sum_k P^*(\mathbf{r}-\mathbf{R}_k)\psi_{c,n}(\mathbf{r},\mathbf{R}_k)}{\sum_k |P(\mathbf{r}-\mathbf{R}_k)|^2} \tag{3}$$

If we want to calculate the guessed object, we calculate

$$O_{g,n+1}(\mathbf{r}) = \begin{cases} \dfrac{\sum_k P^*(\mathbf{r}-\mathbf{R}_k)\psi_{g,n}(\mathbf{r},\mathbf{R}_k)}{\sum_j |P(\mathbf{r}-\mathbf{R}_k)|^2} & \text{for } \sum_k |P(\mathbf{r}-\mathbf{R}_k)|^2 \geq \alpha, \\ 0 & \text{for } \sum_k |P(\mathbf{r}-\mathbf{R}_k)|^2 < \alpha. \end{cases} \quad (4)$$

Here, α is a small parameter.

Simultaneous HIO-PIE:

1. We have a guess for the exit wave functions $\psi_{g,n}(\mathbf{r},\mathbf{R}_j)$ for all probe positions $\mathbf{R}_j$.
2. We calculate the corrected guess for the exit wave functions $\psi_{c,n}(\mathbf{r},\mathbf{R}_j)$ for all probe positions $\mathbf{R}_j$ using steps 3–5 of Sequential PIE.
3. We calculate the object update function

$$U_n(\mathbf{r},\mathbf{R}_j) = P(\mathbf{r}-\mathbf{R}_j)\frac{\sum_k P^*(\mathbf{r}-\mathbf{R}_k)\psi_{c,n}(\mathbf{r},\mathbf{R}_k)}{\sum_k |P(\mathbf{r}-\mathbf{R}_k)|^2} \quad (5)$$

4. We calculate the feedback function

$$B_n(\mathbf{r},\mathbf{R}_j) = b_n(\mathbf{r},\mathbf{R}_j) - P(\mathbf{r}-\mathbf{R}_j)\frac{\sum_k P^*(\mathbf{r}-\mathbf{R}_k)b_n(\mathbf{r},\mathbf{R}_k)}{\sum_k |P(\mathbf{r}-\mathbf{R}_k)|^2}, \quad (6)$$

where

$$b_n(\mathbf{r},\mathbf{R}_j) = \psi_{g,n}(\mathbf{r},\mathbf{R}_j) - \beta\psi_{c,n}(\mathbf{r},\mathbf{R}_j). \quad (7)$$

Here β is HIO feedback parameter and chosen to be 0.9.

5. We obtain new estimates for the exit wave functions using

$$\psi_{g,n+1}(\mathbf{r},\mathbf{R}_j) = U_n(\mathbf{r},\mathbf{R}_j) + B_n(\mathbf{r},\mathbf{R}_j). \quad (8)$$

If we want to calculate the guessed object, we use Eq. (4). Notice that from Eqs. (6) and (8) we can see that feedback information is added to the estimated exit wave. This is where fundamentally our method of Sequential HIO-PIE differs, since we keep the feedback information strictly separated from the object estimate.

2.1. Extension to fPIE

These four algorithms can be straightforwardly extended to fPIE [13]. In this case we undersample the intensity measurements obtained in the diffraction plane: instead of $|\Psi(\mathbf{k},\mathbf{R})|$ we measure $|\Psi(\mathbf{k},\mathbf{R})|\mathbf{III}_\Delta(\mathbf{k})$ where $\mathbf{III}_\Delta(\mathbf{k})$ is a 2D Dirac-comb with period Δ. For fPIE we have to apply the amplitude constraint only to the points in which we have measured $|\Psi(\mathbf{k},\mathbf{R})|$, while we let the other points 'float' freely. More precisely, step 3 of the PIE algorithm would change to

$$\Psi_{c,n}(\mathbf{k},\mathbf{R}) = \begin{cases} \Psi_{g,n}(\mathbf{k},\mathbf{R}) & \text{if } \mathbf{III}_\Delta(\mathbf{k}) = 0, \\ \dfrac{\Psi_{g,n}(\mathbf{k},\mathbf{R})}{|\Psi_{g,n}(\mathbf{k},\mathbf{R})|}|\Psi(\mathbf{k},\mathbf{R})| & \text{if } \mathbf{III}_\Delta(\mathbf{k}) = 1. \end{cases} \quad (9)$$

The other three algorithms change accordingly. Being able to extend the algorithm to fPIE is highly relevant in for example single-shot ptychography [18]. In this case, multiple diffraction patterns are measured simultaneously with one camera, so the sampling rate for each diffraction pattern is reduced.

2.2. Extension to ePIE

One could also try to combine HIO with ePIE, in which case one tries to reconstruct both the object and the probe simultaneously [11]. Because in this case the probe and the object play the same role ($O(\mathbf{r})$ and $P(\mathbf{r})$ can be interchanged without consequence), it makes sense to introduce feedback functions for both the object and the probe.

Regular ePIE

1. We start with the n^{th} guessed object $O_{g,n}(\mathbf{r})$ and n^{th} guessed probe $P_{g,n}(\mathbf{r})$.
2. For a certain probe position $\mathbf{R}$ we calculate the guessed and corrected exit wave according to steps 2–5 of Sequential PIE.
3. We update the guessed object using

$$O_{g,n}(\mathbf{r}) := O_{g,n}(\mathbf{r}) + \frac{P^*_{g,n}(\mathbf{r}-\mathbf{R})}{\max|P_{g,n}(\mathbf{r}-\mathbf{R})|^2}(\psi_{c,n}(\mathbf{r}) - \psi_{g,n}(\mathbf{r})). \quad (10)$$

4. For the same probe position $\mathbf{R}$ we calculate the guessed exit wave $\psi_{g,n}(\mathbf{r}) = P_{g,n}(\mathbf{r})O(\mathbf{r}+\mathbf{R})$ (where $O(\mathbf{r})$ has not yet been updated by Eq. (10)), and correct it according to steps 3–5 of Sequential PIE.
5. We update the guessed probe using

$$P_{g,n}(\mathbf{r}) := P_{g,n}(\mathbf{r}) + \frac{O^*_{g,n}(\mathbf{r}+\mathbf{R})}{\max|O_{g,n}(\mathbf{r}+\mathbf{R})|^2}(\psi_{c,n}(\mathbf{r}) - \psi_{g,n}(\mathbf{r})). \quad (11)$$

6. Once we have done this for all probe positions $\mathbf{R}$, an iteration is completed and we can set $O_{g,n+1}(\mathbf{r}) = O_{g,n}(\mathbf{r})$, $P_{g,n+1}(\mathbf{r}) = P_{g,n}(\mathbf{r})$.

HIO-ePIE

1. We start with the n^{th} guessed object $O_{g,n}(\mathbf{r})$, the n^{th} guessed probe $P_{g,n}(\mathbf{r})$, the n^{th} feedback function for the object $B_{O,n}(\mathbf{r},\mathbf{R})$ for all probe positions $\mathbf{R}$, and the n^{th} feedback function for the probe $B_{P,n}(\mathbf{r},\mathbf{R})$ for all probe positions $\mathbf{R}$.
2. For a certain probe position $\mathbf{R}$ we calculate the guessed exit wave $\psi_{g,n}(\mathbf{r},\mathbf{R}) = O_{g,n}(\mathbf{r})P(\mathbf{r}-\mathbf{R})$.
3. We calculate the guessed diffracted field $\Psi_{g,n}(\mathbf{k},\mathbf{R}) = \mathcal{F}\{\psi_{g,n}(\mathbf{r},\mathbf{R}) + B_{O,n}(\mathbf{r},\mathbf{R})\}$.
4. We obtain a corrected guess for the exit wave function $\psi_{c,n}(\mathbf{r},\mathbf{R})$ as in steps 4–5 of Sequential PIE.
5. We update the guessed object using Eq. (10).
6. We update $B_{O,n}(\mathbf{r})$ according to

$$B_{O,n+1}(\mathbf{r},\mathbf{R}) = \begin{cases} 0 & \text{if } \dfrac{|P_{g,n}(\mathbf{r}-\mathbf{R})|}{\max|P_{g,n}(\mathbf{r}-\mathbf{R})|} \geq \alpha, \\ B_{O,n}(\mathbf{r},\mathbf{R}) - \beta\psi_{c,n}(\mathbf{r},\mathbf{R}) & \text{if } \dfrac{|P_{g,n}(\mathbf{r}-\mathbf{R})|}{\max|P_{g,n}(\mathbf{r}-\mathbf{R})|} < \alpha. \end{cases} \quad (12)$$

Here α is a small parameter, and β is the HIO feedback parameter which we choose to be 0.9.

7. For the same position $\mathbf{R}$ we calculate the guessed exit wave $\psi_{g,n}(\mathbf{r},\mathbf{R}) = O_{g,n}(\mathbf{r}+\mathbf{R})P(\mathbf{r})$. Note that we use for convenience the same notation $\psi_{g,n}(\mathbf{r},\mathbf{R})$ as in step 2, even though these two functions are not identical.
8. We calculate the guessed diffracted field $\Psi_{g,n}(\mathbf{k},\mathbf{R}) = \mathcal{F}\{\psi_{g,n}(\mathbf{r},\mathbf{R}) + B_{P,n}(\mathbf{r},\mathbf{R})\}$.
9. We obtain a corrected guess for the exit wave function $\psi_{c,n}(\mathbf{r},\mathbf{R})$ as in steps 4–5 of Sequential PIE.
10. We update the guessed probe using Eq. (11).
11. We update $B_{P,n}(\mathbf{r})$ according to

$$B_{P,n+1}(\mathbf{r},\mathbf{R}) = \begin{cases} 0 & \text{if } \dfrac{|O_{g,n}(\mathbf{r}+\mathbf{R})|}{\max|O_{g,n}(\mathbf{r}+\mathbf{R})|} \geq \alpha, \\ B_{P,n}(\mathbf{r},\mathbf{R}) - \beta\psi_{c,n}(\mathbf{r},\mathbf{R}) & \text{if } \dfrac{|O_{g,n}(\mathbf{r}+\mathbf{R})|}{\max|O_{g,n}(\mathbf{r}+\mathbf{R})|} < \alpha. \end{cases} \quad (13)$$

Here α is a small parameter, and β is the HIO feedback parameter which we choose to be 0.9.

(a) Object amplitude

(b) Object phase

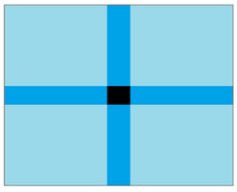

(c) 10% probe overlap.

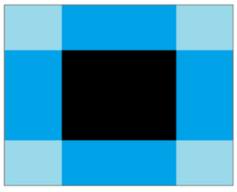

(d) 50% probe overlap.

(e) 90% probe overlap.

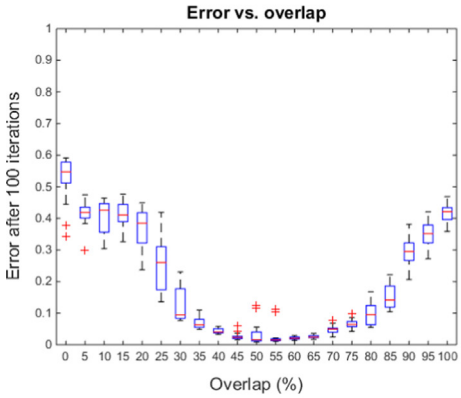

(f) Sequential (regular) PIE

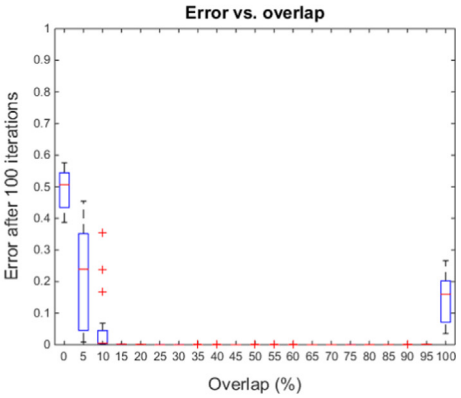

(g) Sequential HIO-PIE.

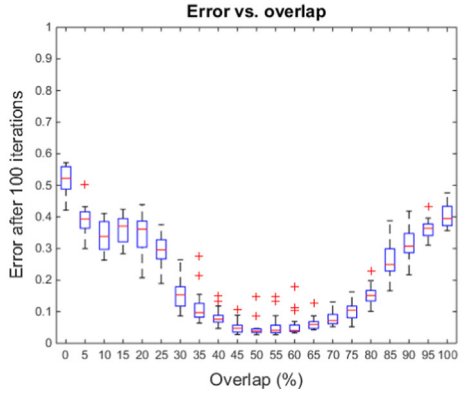

(h) Simultaneous PIE

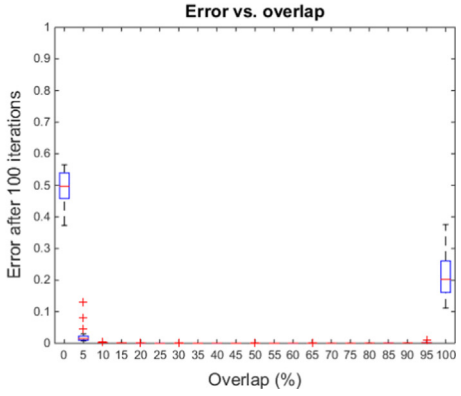

(i) Simultaneous HIO-PIE.

Fig. 2. Top row: the complex-valued test object used for reconstruction. The phase spans a range of $0.7 \cdot 2\pi$. Second row: varying the amount of overlap between the 2×2 probe positions that are used to obtain the intensity measurements in the diffraction plane. Bottom four plots: reconstruction errors after 100 iterations for the four different algorithms as a function of the overlap between probe positions. For each value of overlap, the statistics (median, first and third quartile, minimum and maximum, and outliers) for 20 different random initial guesses are plotted.

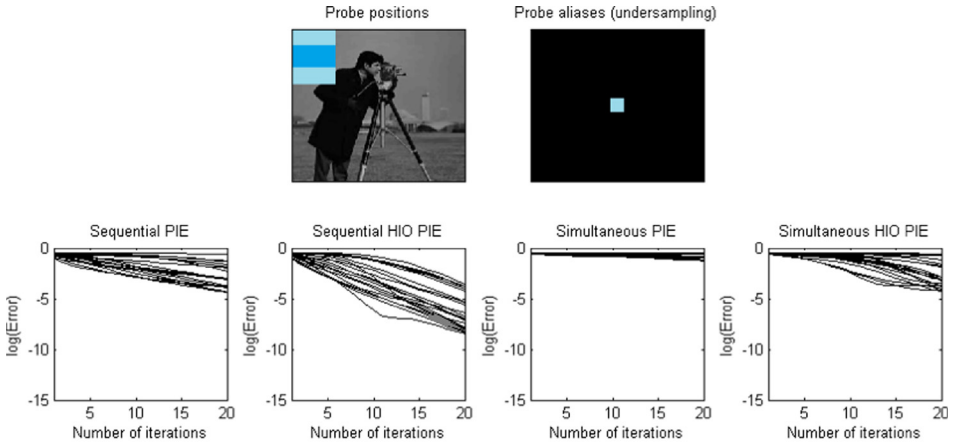

(a) **Case 1:** 8×8 probe positions, probe dimensions = 25% object dimensions (58% probe overlap), no undersampling.

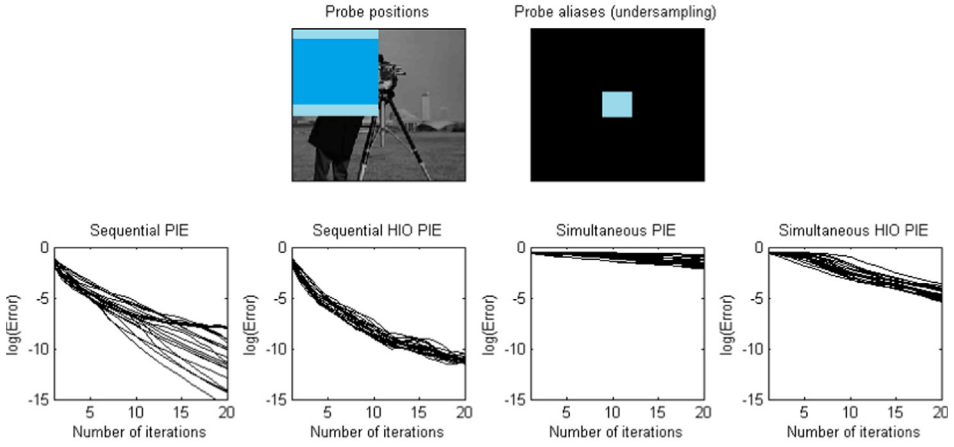

(b) **Case 2:** 8×8 probe positions, probe dimensions = 50% object dimensions (86% probe overlap), no undersampling.

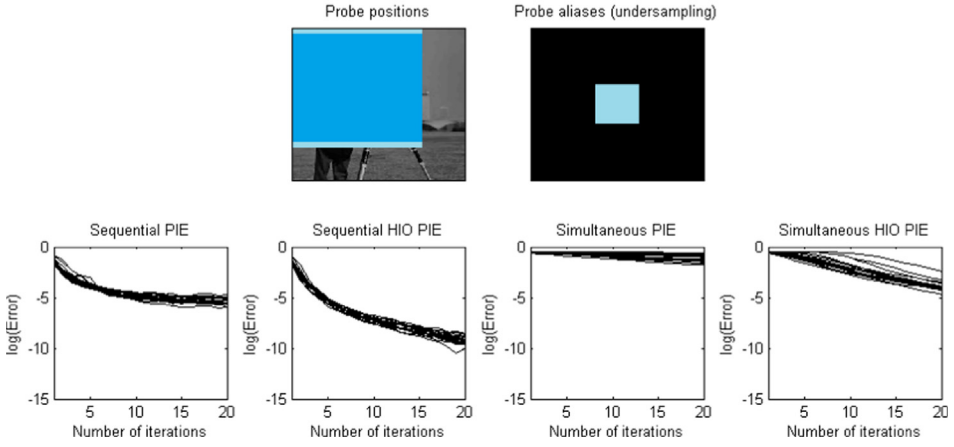

(c) **Case 3:** 8×8 probe positions, probe dimensions = 75% object dimensions (95% probe overlap), no undersampling

Fig. 3. Comparison of the four algorithms for 8×8 probes. The blue squares represent the positions of two adjacent probes, and the dark blue region indicates where they overlap. The error plots show the evolution of the reconstruction error for 20 different random initial guesses (random phase, random amplitude). (For interpretation of the references to color in this figure legend, the reader is referred to the web version of this article.)

3. Simulation results

For all simulations we use a complex-valued test object that is shown in Fig. 2a and b.

3.1. No undersampling

For the first simulation, we see how the four algorithms perform in the case shown in Fig. 2(c)–(e): the probe $P(\mathbf{r})$ is a square step function that is shifted to four positions $\mathbf{R}$. Simulations are performed for different amounts of overlap. Since we are keeping the total field of view constant, we need to vary the probe size as we vary the overlap. The initial guessed object has random amplitude and random phase. Because for each different initial guess the algorithms may converge differently, we have performed the algorithm 20 times with different initial guesses for each value of overlap. In Fig. 2 it is shown how for each algorithm, the reconstruction error changes with the amount of overlap between the probes. Note that 'one iteration' means going through all the probe positions $\mathbf{R}$ once. The results show that for this case, separated HIO-PIE is by far more reliable. The functional we have used to characterize the reconstruction error is

$$E[O_{g,n}(\mathbf{r})] = \frac{\int |O(\mathbf{r}) - cO_{g,n}(\mathbf{r})|^2 \, \mathrm{d}\mathbf{r}}{\int |O(\mathbf{r})|^2 \, \mathrm{d}\mathbf{r}}. \tag{14}$$

Here, c is a complex constant that minimizes E. This assures that if $O_{g,n}(\mathbf{r}) = e^{i\theta}O(\mathbf{r})$, the error is 0 as it should be. c is found by solving $\mathrm{d}E/\mathrm{d}c = 0$, which gives

$$c^* = \frac{\int O^*(\mathbf{r}) O_{g,n}(\mathbf{r}) \, \mathrm{d}\mathbf{r}}{\int |O_{g,n}(\mathbf{r})|^2 \, \mathrm{d}\mathbf{r}}. \tag{15}$$

In the next simulation, we compare the four different algorithms for the case where we use 8×8 probe positions. The reconstruction results for three different probe sizes are shown in Fig. 3. For each case, we plot the evolution of the reconstruction for twenty runs of the algorithm, each with a different random initial guess (random phase and random amplitude distribution). It can be seen that in nearly all situations our proposed method of Sequential HIO-PIE is at least as good as the other methods, and often even significantly outperforming them.

3.2. Effect of shot noise

Simulations have been performed to investigate the PIE and HIO-PIE algorithms in case the intensity measurements are affected by shot noise (i.e. Poisson noise). To simulate the shot noise, all the simulated intensity patterns are multiplied by a certain gain factor such that the total photon count of each measurement lies around a certain value (in this case either 10^4, 10^5, 10^6, 10^7, or 10^8). To simulate a measurement affected by shot noise, each pixel is assigned a value obtained by taking a sample from a Poisson distribution, the mean value of which is the value of that pixel in the noise-free case. It was noted in [19] that HIO may fail to converge to the right solution when shot noise is present, and that the algorithm needs to be adapted in order to make it work. In [15], it was noted that it usually is beneficial to alternate between iterations of ER and iterations of HIO. In a similar vein, to deal with the presence of shot noise we propose a scheme of a slightly modified HIO-PIE (let us call it snHIO-PIE, where sn is short for shot noise), in which also the intensity measurements are updated, and in which we alternatingly use HIO-PIE iterations and PIE iterations.

snHIO-PIE

- Apply 20 HIO-PIE iterations. Each time the object estimate $O_g(\mathbf{r})$ is updated, also update the estimated intensity pattern $I_g(\mathbf{k}, \mathbf{R})$ as follows

$$I_g(\mathbf{k}, \mathbf{R}) := \begin{cases} |\Psi_g(\mathbf{k}, \mathbf{R})|^2 & \text{if } |I_{\text{noise}}(\mathbf{k}, \mathbf{R}) - |\Psi_g(\mathbf{k}, \mathbf{R})|^2| < 2|\Psi_g(\mathbf{k}, \mathbf{R})|, \\ I_{\text{noise}}(\mathbf{k}, \mathbf{R}) & \text{otherwise.} \end{cases} \tag{16}$$

  Here, $\Psi_g(\mathbf{k}, \mathbf{R}) = \mathcal{F}\{O_g(\mathbf{r})P(\mathbf{r} - \mathbf{R})\}$, and $I_{\text{noise}}(\mathbf{k}, \mathbf{R})$ is the measured intensity pattern, that is affected by Poisson noise. The idea behind this update is that the noisy measurement I_{noise} is not expected to deviate from the noise-free intensity pattern I by more than two times the standard deviation of a Poisson distribution with a mean value of I. This standard deviation is $\sqrt{I}$, so in short we expect $|I_{\text{noise}} - I| < 2\sqrt{I}$. For the HIO-PIE iterations, $I_g(\mathbf{k}, \mathbf{R})$ are used for the amplitude constraints.
- Apply 20 PIE iterations. For the amplitude constraints, $I_{\text{noise}}(\mathbf{k}, \mathbf{R})$ are used. Set the HIO feedback functions $B(\mathbf{r}, \mathbf{R})$ to 0, and update $I_g(\mathbf{k}, \mathbf{R})$ as in Eq. (16).
- Repeat the above two steps.

The results of this scheme are shown in Fig. 4. For the simulations, we used 2×2 probes with 60% overlap, which is according to the results of Fig. 2 the optimal value of overlap for PIE for this setting. For low levels of noise, the reconstruction error is significantly lower for snHIO-PIE, which is to be expected from the results of Fig. 2. For higher levels of noise, the difference in reconstruction error decreases. However, even when the noise level is so high that the reconstruction errors are practically the same for both methods, snHIO-PIE appears to converge faster, which is beneficial when computing time is of the essence (e.g. if the reconstruction takes place as part of a feedback-loop).

3.3. With undersampling

We have also performed simulations on how the four algorithms perform when they are extended to fPIE. The three cases in which now the intensity measurements in the diffraction plane are undersampled are shown in Fig. 5. The rate of undersampling is illustrated by the aliases of the probe obtained by calculating $\mathcal{F}^{-1}\{\mathcal{F}\{P(\mathbf{r})\}\mathbf{III}_{\Delta}(\mathbf{k})\}$: if the probe $P(\mathbf{r})$ is Fourier transformed and sampled in Fourier space, then its inverse Fourier transform will consist of displaced copies of $P(\mathbf{r})$. The distance between these copies decrease when the sampling interval is increased, thus from the locations of these copies one can infer the sampling interval in Fourier space. In particular, if the copies of $P(\mathbf{r})$ overlap, it means the sampling is sub-Nyquist. In this case, separating the feedback function seems essential in order to obtain a good reconstruction.

3.4. Probe and object reconstruction

A very important variation of the PIE algorithm is ePIE, which reconstructs both the probe function and the object function simultaneously. Since the probe is also being reconstructed, the object reconstruction will not deteriorate due to unknown aberrations in the probe. In this section, we investigate the effects augmenting the ePIE algorithm with HIO. To simulate a realistic scenario, we choose the probe to a circular step function (as would be created by an aperture) with some aberrations (in this case we choose astigmatism) that is propagated over a small distance. The initial guess we use for the probe is the unaberrated, unpropagated circular step function. This is shown in Fig. 6. The initial guesses we use for the object functions have random amplitude and random phase.

First, we compare ePIE with HIO-ePIE as described in Eqs. (12) and (13) for the noise-free case. For the first ten iterations, the probe estimate is not updated for either algorithm. The results for 3×3 probe positions and 6×6 probe positions are shown in

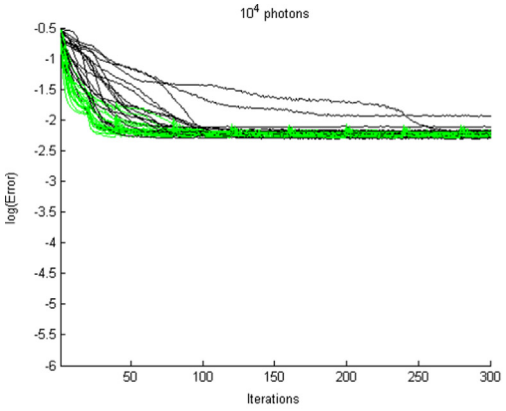

(a) 10^4 photons, 2×2 probe positions, 60% probe overlap, $\bar{E}_{\text{PIE}} = 0.1103$, $\bar{E}_{\text{snHIO-PIE}} = 0.1071$.

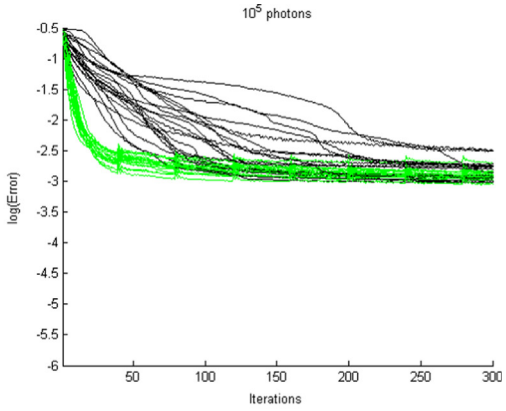

(b) 10^5 photons, 2×2 probe positions, 60% probe overlap, $\bar{E}_{\text{PIE}} = 0.0593$, $\bar{E}_{\text{snHIO-PIE}} = 0.0536$.

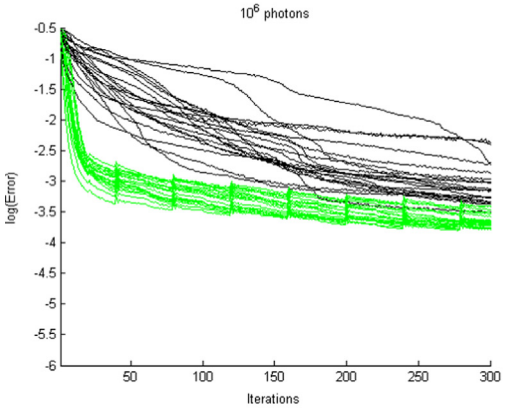

(c) 10^6 photons, 2×2 probe positions, 60% probe overlap, $\bar{E}_{\text{PIE}} = 0.0489$, $\bar{E}_{\text{snHIO-PIE}} = 0.0264$.

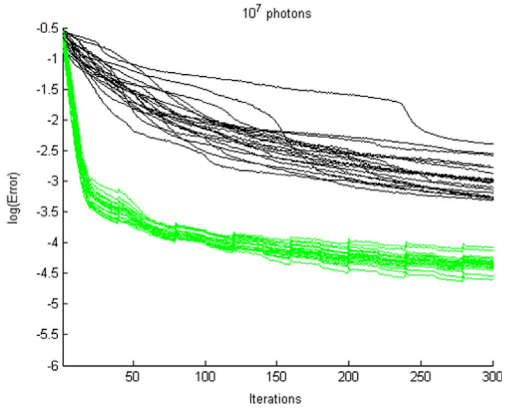

(d) 10^7 photons, 2×2 probe positions, 60% probe overlap, $\bar{E}_{\text{PIE}} = 0.0516$, $\bar{E}_{\text{snHIO-PIE}} = 0.0131$.

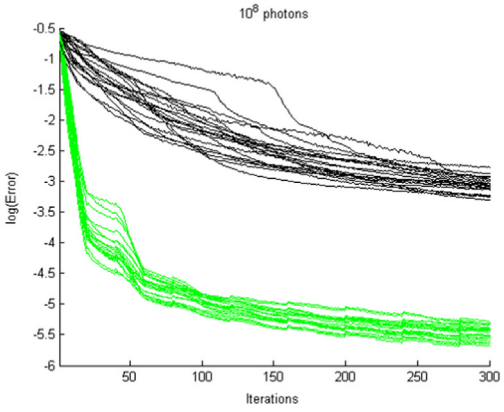

(e) 10^8 photons, 2×2 probe positions, 60% probe overlap, $\bar{E}_{\text{PIE}} = 0.0471$, $\bar{E}_{\text{snHIO-PIE}} = 0.0042$.

Fig. 4. Comparison of the PIE (black) and HIO-PIE (green) algorithms in the presence of different levels of Poissonian shot noise. For each noise level, 20 runs have been performed for each algorithm. The error plots show the evolution of the reconstruction error for 20 different random initial guesses (random phase, random amplitude) and different noise patterns for each algorithm. $\bar{E}_{\text{PIE}}$ and $\bar{E}_{\text{snHIO-PIE}}$ denote the average reconstruction error (as defined in Eq. (14)) after 300 iterations for PIE and snHIO-PIE respectively. (For interpretation of the references to color in this figure legend, the reader is referred to the web version of this article.)

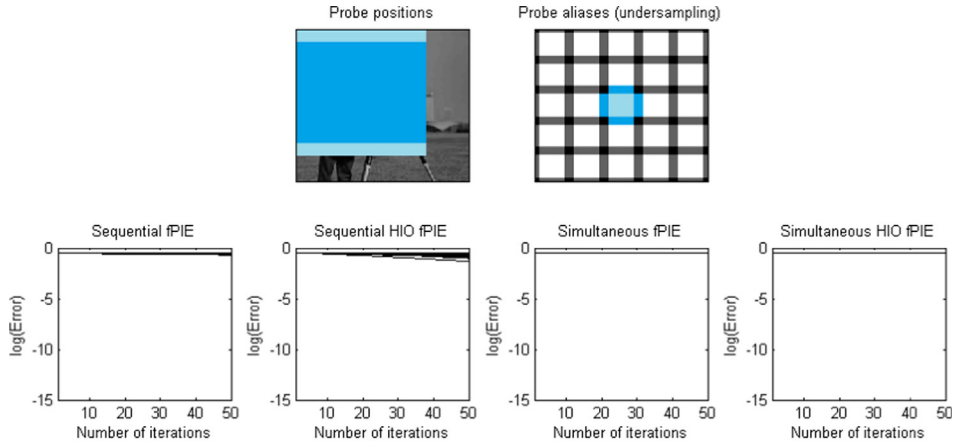

(a) **Case 4:** 4×4 probe positions, probe dimensions = 75% object dimensions (89% probe overlap), $\omega_{\text{sample}} = 0.8\omega_{\text{Nyquist}}$.

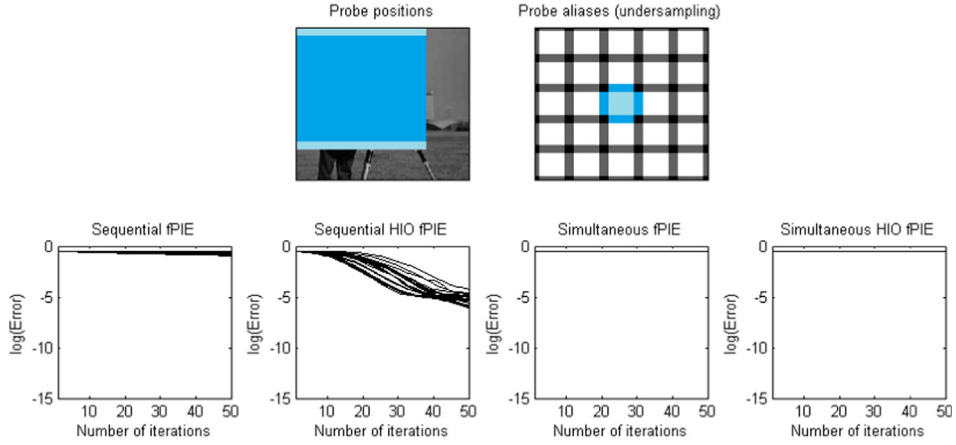

(b) **Case 5:** 6×6 probe positions, probe dimensions = 75% object dimensions (93% probe overlap), $\omega_{\text{sample}} = 0.8\omega_{\text{Nyquist}}$.

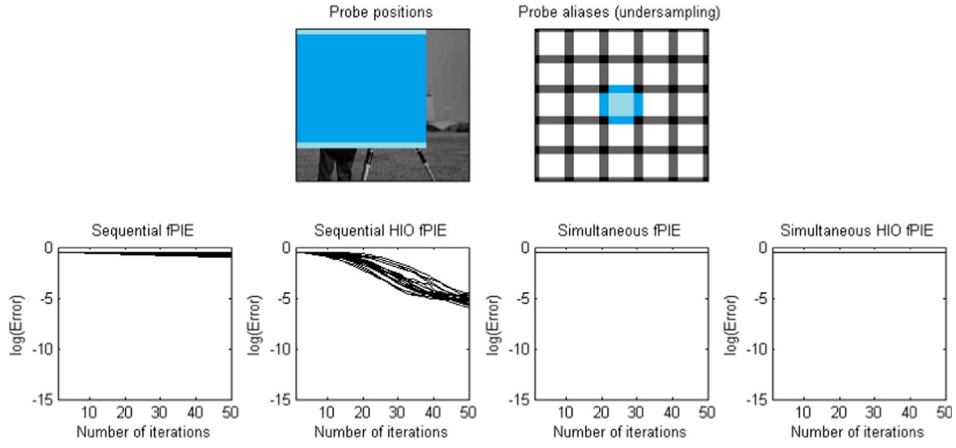

(c) **Case 6:** 8×8 probe positions, probe dimensions = 75% object dimensions (95% probe overlap), $\omega_{\text{sample}} = 0.8\omega_{\text{Nyquist}}$.

Fig. 5. Comparison of the four algorithms (extended to their fPIE version) for different numbers of probes, with a constant probe size. The blue squares represent the positions of two adjacent probes, and the dark blue region indicates where they overlap. The sampling frequency ω_{sample} is proportional to $1/\Delta$, where Δ is the sampling interval as used in Eq. (9).The error plots show the evolution of the reconstruction error for 20 different random initial guesses (random phase, random amplitude). (For interpretation of the references to color in this figure legend, the reader is referred to the web version of this article.)

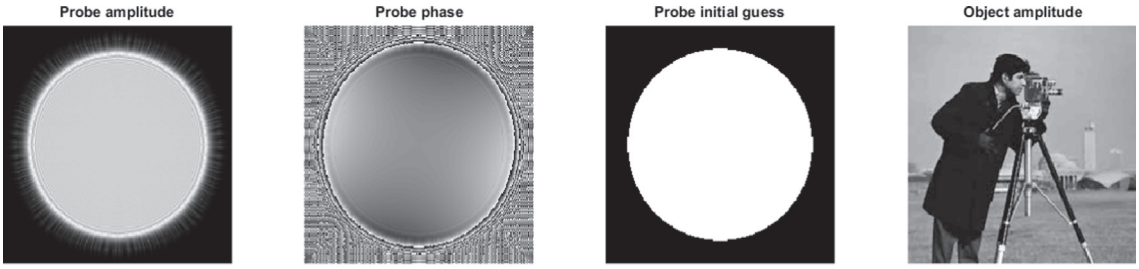

(a) The probe and the initial guess for the probe used in the (HIO-)ePIE simulations. The probe and the object have the same scale.

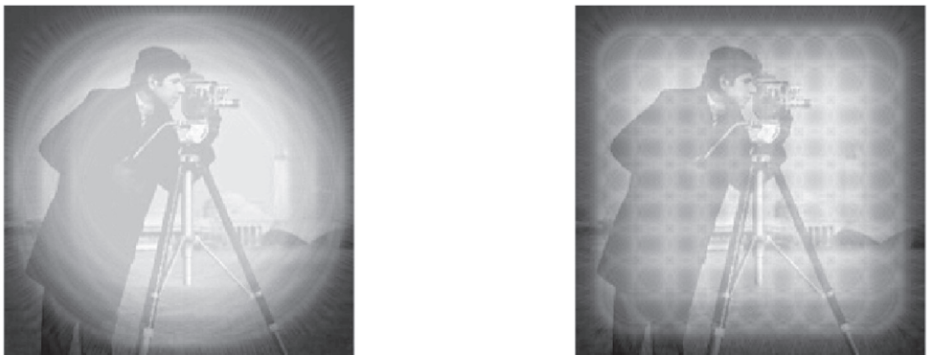

(b) 3×3 large probes on the object's amplitude(c) 8×8 small probes on the object's amplitude

Fig. 6. Illustration of the probes used for simulating (HIO-)ePIE.

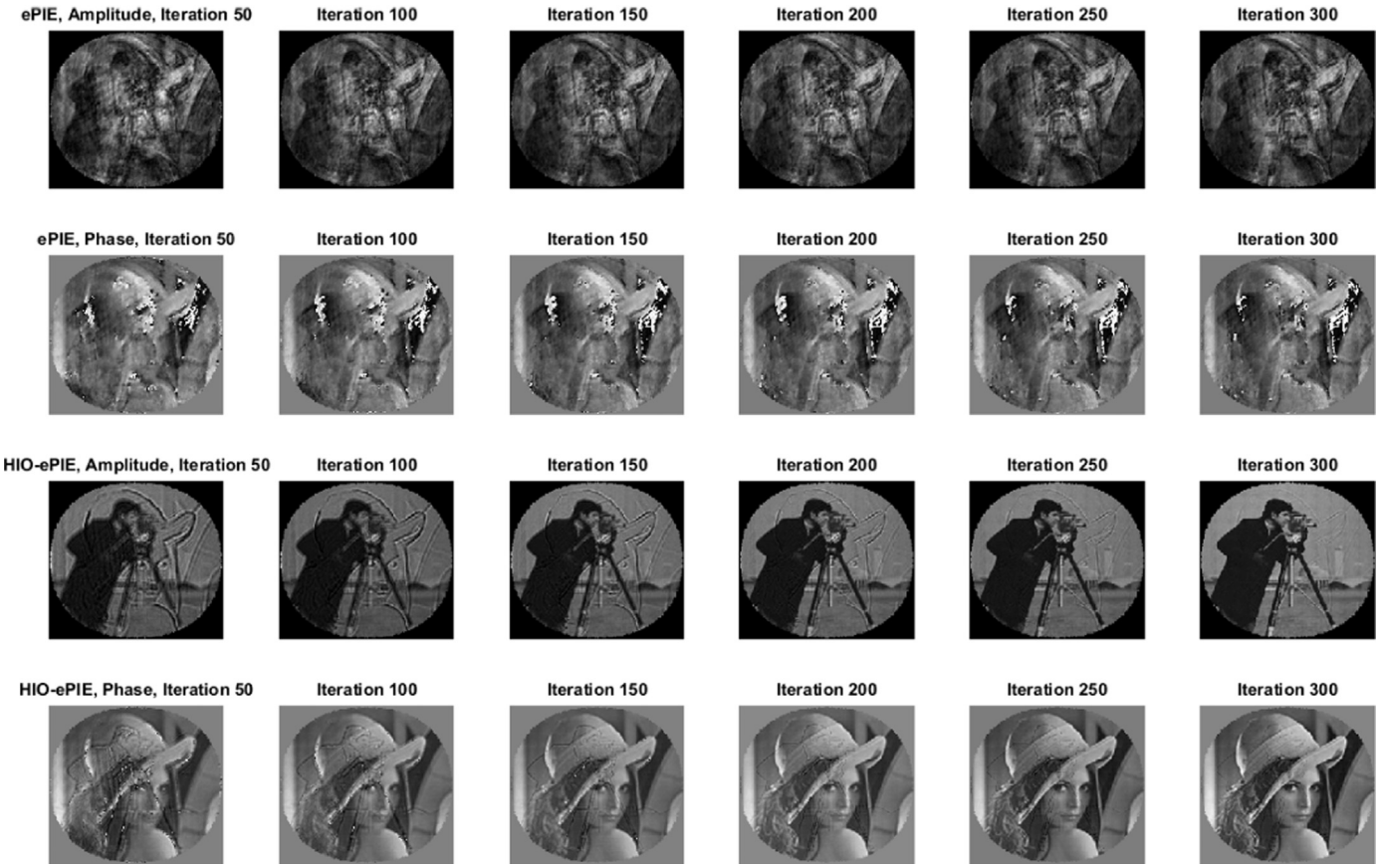

Fig. 7. Reconstruction for ePIE and HIO-ePIE in the noise-free case, with 3×3 large probes.

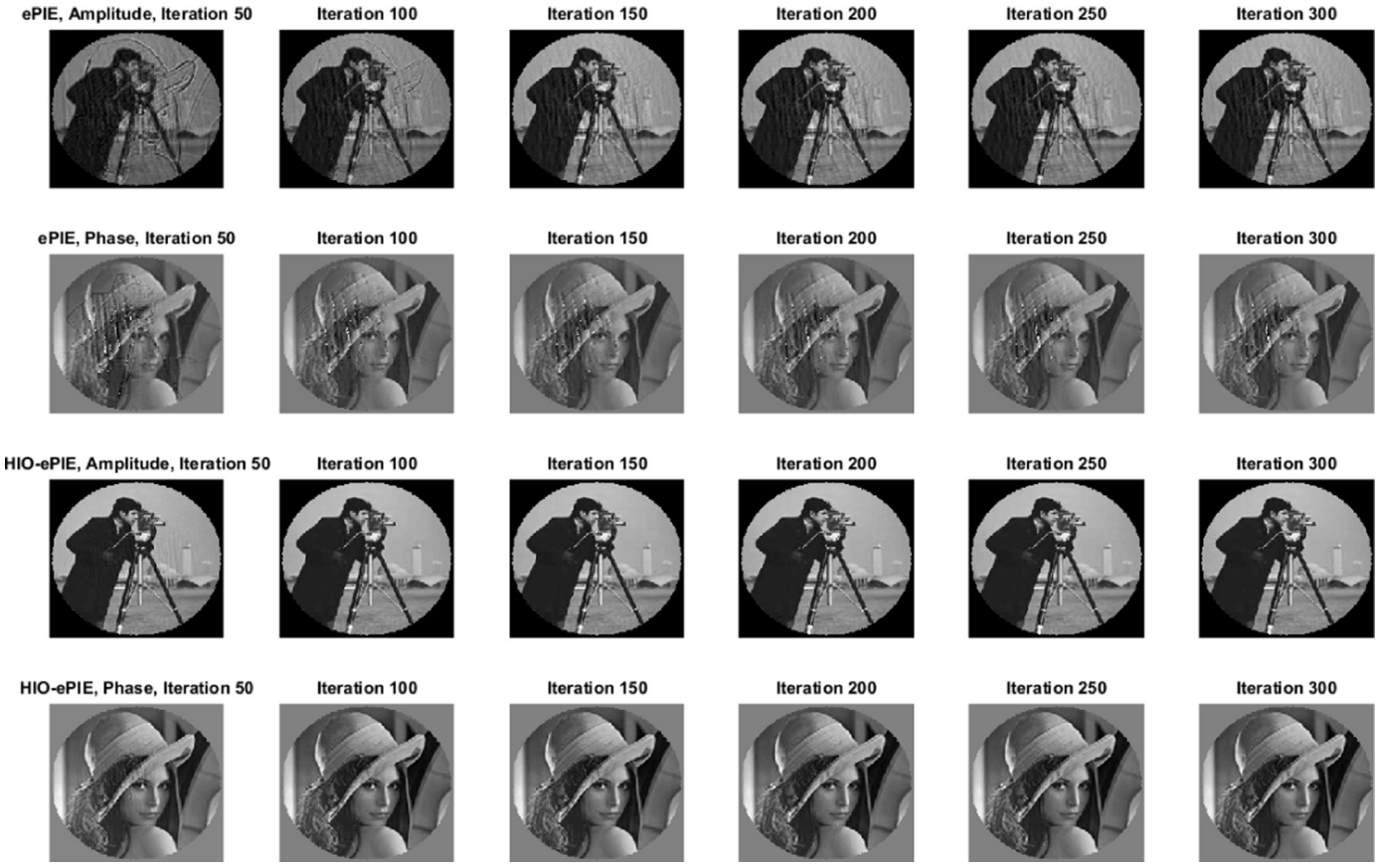

Fig. 8. Reconstruction for ePIE and HIO-ePIE in the noise-free case, with 6×6 large probes.

Fig. 9. Reconstruction for ePIE and HIO-ePIE in the noise-free case, with 8×8 small probes.

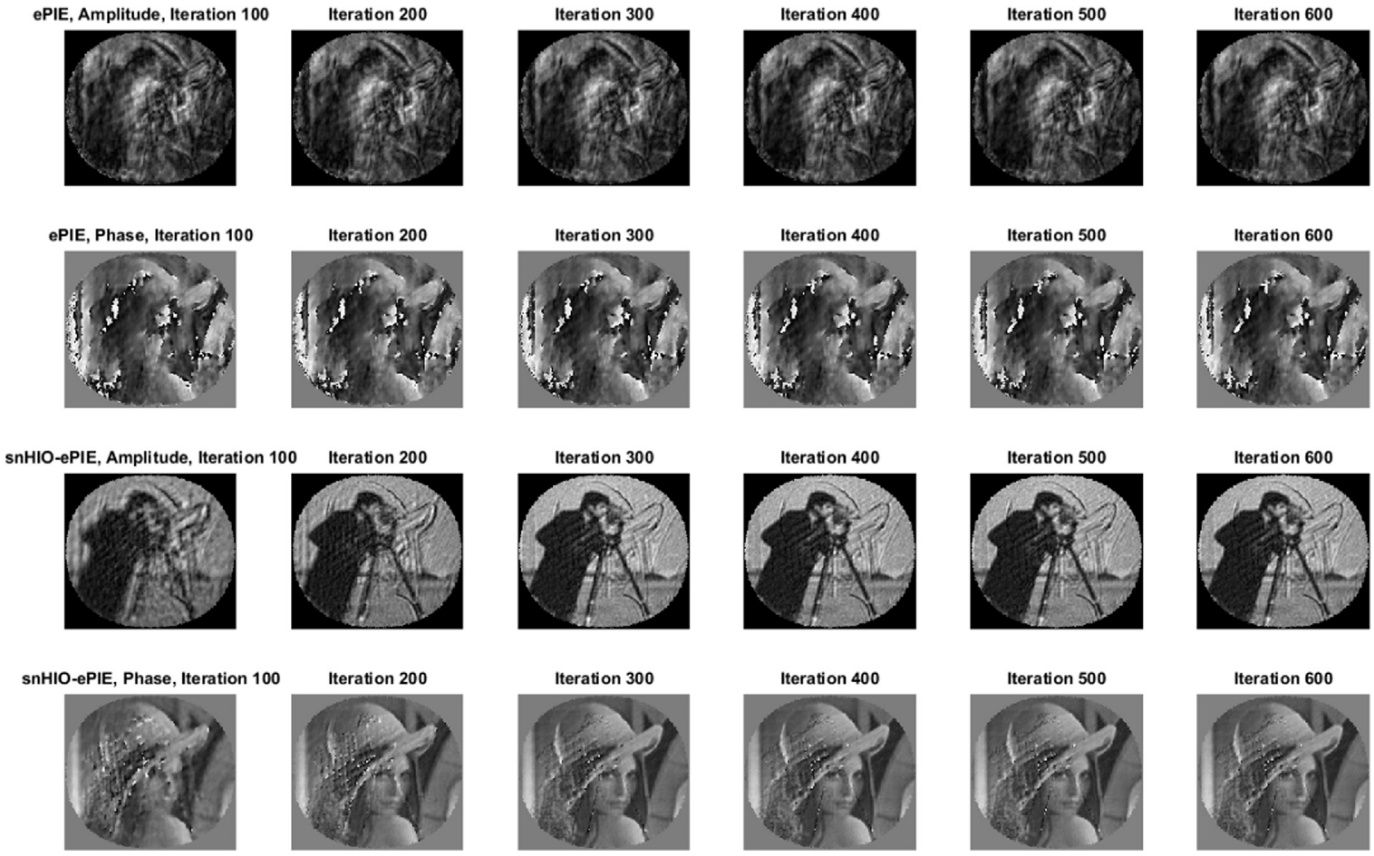

Fig. 10. Reconstruction for ePIE and HIO-ePIE in the presence of shot noise, with 3×3 large probes.

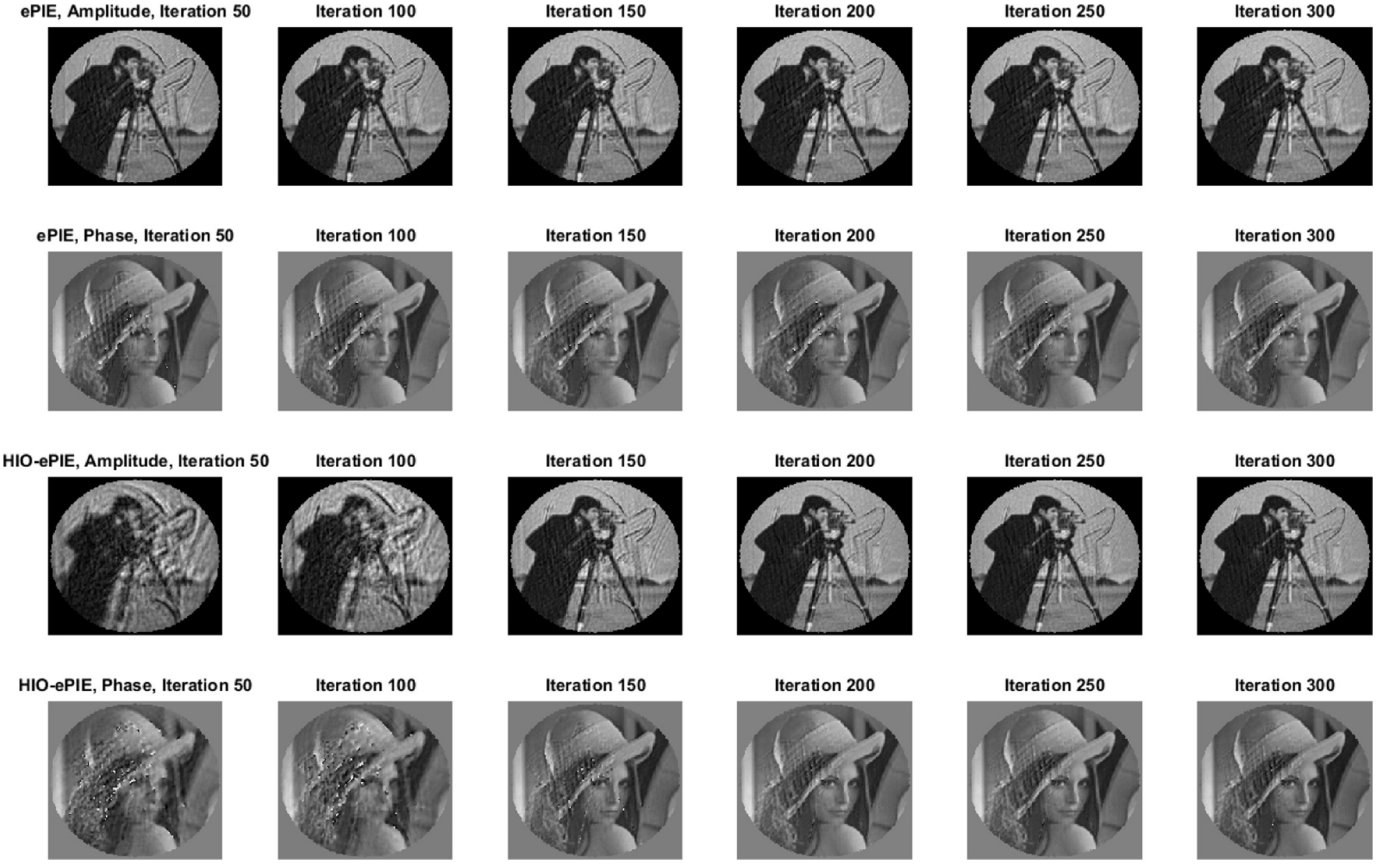

Fig. 11. Reconstruction for ePIE and HIO-ePIE in the presence of shot noise, with 6×6 large probes.

Figs. 7 and 8 respectively. It is shown that when large probes are used, the reconstruction obtained with the regular ePIE algorithm contains noticeable artifacts. Especially when fewer probe positions, namely 3×3, are used, the difference between ePIE and HIO-ePIE becomes even more apparent. When we use smaller probes as in Fig. 9, the reconstruction of regular ePIE contains no noticeable artifacts. However, HIO-ePIE converges faster in this noise-free case.

Next, we study the case in which the intensity measurements are affected by shot noise. The intensity measurements have total photon counts of approximately 10^6. In the presence of shot noise it is required to extend HIO-ePIE like HIO-PIE was extended to snHIO-PIE as in Eq. (16). That is, the intensity measurements have to be reconstructed, and one has to alternate between HIO-ePIE iterations and regular ePIE iterations. Additionally, simulations have shown it to be beneficial to introduce a cut-off value σ for the HIO feedback functions $B_O(\mathbf{r}, \mathbf{R})$ and $B_P(\mathbf{r}, \mathbf{R})$ as was proposed in [19]. That is, during each iteration we set

$$B_n(\mathbf{r}, \mathbf{R}) = \begin{cases} B_n(\mathbf{r}, \mathbf{R}) & \text{if } |B_n(\mathbf{r}, \mathbf{R})| > \sigma, \\ 0 & \text{if } |B_n(\mathbf{r}, \mathbf{R})| \leq \sigma. \end{cases} \tag{17}$$

Here, σ is some cut-off value that depends on the noise level. It basically indicates which values of $B_n(\mathbf{r}, \mathbf{R})$ are sufficiently small such that they can be non-zero due to noise. In the case of noise-free measurements, σ would be reduced to 0. The result for 3×3 probes is shown in Fig. 10, where one can see that the effect of augmenting ePIE with HIO is significant. When using 6×6 probes, as shown in Fig. 11, the differences between the reconstructions are much less pronounced.

4. Conclusions

In this article we have proposed a way to combine existing ptychographical algorithms such as PIE, ePIE and fPIE with the HIO algorithm. Simulations indicate that for many instances the combination with HIO results in a considerable improvement. In the noise-free case, an extension with HIO is almost always an improvement, though when shot noise is present in the algorithm, extra adaptions have to be applied to the algorithm. Nevertheless, when few probe positions are used, the HIO-augmented algorithms still tend to produce reconstructions that are noticeably better and obtained in fewer iterations than those obtained by the unaugmented algorithms. As the number of probes is increased and shot noise is introduced, the difference between the reconstructions of the two algorithms becomes smaller. Although we have focused here on the HIO algorithm, the same train of thought can be applied more generally: when combining any ptychographical algorithm with some other algorithm that uses a feedback function, this function ought be kept strictly separate from the object function. Hopefully with this insight, many ptychographical algorithms can be improved significantly in a straightforward manner.

References

[1] R.W. Gerchberg, Optik 35 (1972) 237.
[2] J.R. Fienup, Opt. Lett. 3 (1) (1978) 27–29.
[3] J.P. Abrahams, A.G.W. Leslie, Acta Crystallogr. Sect. D 52 (1) (1996) 30–42.
[4] H.H. Bauschke, P.L. Combettes, D.R. Luke, JOSA A 19 (7) (2002) 1334–1345.
[5] H.H. Bauschke, P.L. Combettes, D.R. Luke, JOSA A 20 (6) (2003) 1025–1034.
[6] D.R. Luke, Inverse Probl. 21 (1) (2004) 37.
[7] J.M. Rodenburg, R.H.T. Bates, Philos. Trans. R. Soc. A 339 (1655) (1992) 521–553.
[8] A.J. D'Alfonso, A.J. Morgan, A.W.C. Yan, P. Wang, H. Sawada, A.I. Kirkland, L. J. Allen, Phys. Rev. B 89 (6) (2014) 064101.
[9] T.J. Pennycook, A.R. Lupini, H. Yang, M.F. Murfitt, L. Jones, P.D. Nellist, Ultramicroscopy 151 (2015) 160–167.
[10] J.M. Rodenburg, H. Faulkner, Appl. Phys. Lett. 85 (20) (2004) 4795–4797.
[11] A.M. Maiden, J.M. Rodenburg, Ultramicroscopy 109 (10) (2009) 1256–1262.
[12] M. Guizar-Sicairos, J.R. Fienup, Opt. Express 16 (10) (2008) 7264–7278.
[13] T.B. Edo, D.J. Batey, A.M. Maiden, C. Rau, U. Wagner, Z.D. Pešić, T.A. Waigh, J. M. Rodenburg, Phys. Rev. A 87 (5) (2013) 053850.
[14] J.R. Fienup, Appl. Opt. 21 (15) (1982) 2758–2769.
[15] S. Marchesini, Rev. Sci. Instrum. 78 (1) (2007) 011301.
[16] J. Qian, C. Yang, A. Schirotzek, F. Maia, S. Marchesini, Inverse Probl. Appl. Contemp. Math. 615 (2014) 261–280.
[17] S. Marchesini, A. Schirotzek, C. Yang, H. Wu, F. Maia, Inverse Probl. 29 (11) (2013) 115009.
[18] P. Sidorenko, O. Cohen, Optica 3 (1) (2016) 9–14.
[19] A.V. Martin, et al., Opt. Express 20 (15) (2012) 16650–16661.